Scripta Materialia 160 (2019) 86–91

Contents lists available at ScienceDirect

Scripta Materialia

journal homepage: www.elsevier.com/locate/scriptamat

Modification of boundary structure and magnetic properties of Nd-Fe-B sintered magnets by diffusing Al/Cu co-added alloy ribbons

Kechao Lu, Xiaoqian Bao *, Guixian Chen, Xuejiao Zhang, Minghui Tang, Xing Mu, Jiheng Li, Xuexu Gao

State Key Laboratory for Advanced Metals and Materials, University of Science and Technology Beijing, 30 Xue Yuan Road, Beijing 100083, People's Republic of China

ARTICLE INFO

Article history:
Received 3 August 2018
Received in revised form 6 September 2018
Accepted 1 October 2018
Available online xxxx

Keywords:
Nd-Fe-B permanent magnet
Wetting
Grain boundary diffusion
Grain boundaries
Coercivity

ABSTRACT

Wetting experiments of $Tb_{70}Cu_{30}$, $Pr_{52.5}Tb_{17.5}Cu_{30}$, $Pr_{60}Tb_{20}Al_{20}$ and $Pr_{60}Tb_{10}Cu_{15}Al_{15}$ (at.%) ingots over Nd-Fe-B sintered magnet were carried out and suggested that alloys containing Al possessed better wettability and mobility. Interfacial analysis suggested that at interface between $Pr_{60}Tb_{20}Al_{20}$ and magnet, Tb mainly diffused along grain boundaries without abnormal Tb-rich grains, which were observed in the systems of Cu-added ingots. On the basis of these, grain boundary diffusion with alloy ribbons was applied and coercivity increment of over 11 kOe was achieved by consuming below 0.5 wt.% Tb in diffused magnet by $Pr_{60}Tb_{10}Cu_{15}Al_{15}$, which was mainly attributed to homogeneous and thin Tb-rich shells.

Nd-Fe-B magnet has shown a record maximum energy product $(BH)_{max}$, but a relatively low coercivity has been the stumbling block for the use in traction motors of (hybrid) electric vehicles, in which the application environment causes dramatical thermal demagnetization [1]. It is generally thought that the coercivity (Hci) of Nd-Fe-B sintered magnet is controlled by nucleation of reversed magnetic domains. During demagnetization, reversed magnetic domains first arise from the local regions at the outer layers of $Nd_2Fe_{14}B$ grain or surface defects adjacent to Nd-rich phases and then propagate across neighboring grains [2]. Therefore, it is crucial to strengthen boundary structure. The magnetocrystalline anisotropy field (H_A) at boundaries could be enhanced by forming a higher anisotropy field of shells rich in heavy rare earth (HRE) elements [3]. It has been extensively reported that core-shells rich in Dy or Tb (HRE) at outer layers of $Nd_2Fe_{14}B$ grains can be constructed by grain boundary diffusion process (GBDP) with pure HRE or HRE compounds, i.e. in the form of vapor [3], oxides [4], fluorides [5,6], hydrides [7,8]. However, due to anti-ferromagnetic coupling of HRE and Fe atoms [9], HRE-rich shells should be controlled to be as thin as possible to balance coercivity enhancement and remanence reduction. Furthermore, finite element micromagnetic simulation has confirmed that 4 nm thick HRE-rich shells are sufficient to cancel out coercivity deterioration caused by defect layers at grain boundaries [10]. So, it is significant to modify the thickness of HRE-rich shells.

Recently, grain boundary diffusion or doping with low melting-point RE-(Cu, Al) alloys has been used to enhance the coercivity of HDDR Nd-Fe-B powders [11], hot-deformed Nd-Fe-B magnets [12,13] and sintered Nd-Fe-B magnets [14–16], which are mainly attributed to magnetic hardening by HRE-rich shells and magnetic isolation enhancement of Nd-rich phases. On the other hand, continuous Nd-rich phases are thought to be critical diffusion channels of Dy or Tb. What's more, Knoch and Goto [17,18] have revealed that addition of Al and Cu into Nd-Fe-B magnet can improve the wettability of Nd-rich phases and therefore optimize boundary structure. Consequently, the introducing of Al and Cu accompanying with Tb is helpful to improve the boundary structure and diffusing behavior of Tb. In this paper, on the basis of the results of wetting experiments and characteristic interfacial reaction, we discussed about the microstructural and magnetic property changes of Nd-Fe-B magnet by diffusing Al/Cu co-added alloy ribbons.

The wettability of $Tb_{70}Cu_{30}$ (TC), $Pr_{52.5}Tb_{17.5}Cu_{30}$ (PTC), $Pr_{60}Tb_{20}Al_{20}$ (PTA) and $Pr_{60}Tb_{10}Cu_{15}Al_{15}$ (PTCA) ingots over commercial N50 magnets (without Dy/Tb) were respectively measured by sessile drop method in the stainless-steel chamber, similar to the description in Ref. [19]. The alloy ingots were prepared by inductively melting in high-vacuum condition. The N50 substrate and alloy ingots with a size of $4 \times 4 \times 4$ mm^3 were polished by abrasive papers and diamond pastes with 1 μm. The experiments were performed at a constant temperature of 900 °C for 30 min under a high vacuum of $(5–6) \times 10^{-4}$ Pa. High-resolution photographs were taken at a maximum speed of 2 frames/s using a charge-coupled device (CCD) camera. In the GBDP experiments, the same N50 magnets were used as the original magnets with a dimensional size of Φ 8 × 5 mm^3, in which the axial direction was parallel to magnetic alignment direction. The TC, PTC and PTCA ribbons were melt-spun with the copper roller speed about 8 m/s. The upper and

* Corresponding author.
E-mail address: bxq118@ustb.edu.cn (X. Bao).

https://doi.org/10.1016/j.scriptamat.2018.10.001
1359-6462/

lower surfaces of cylinder magnet were individually covered by alloy ribbons and set in the ceramic crucible. The GBDP was performed at 900 °C and held for 6 h, following by a subsequent annealing treatment at 500 °C for 2 h. All heat treatments were under the high-vacuum condition (~3×10^{-3} Pa) and cooled by water. The magnetic properties of the diffused magnets were measured by NIM-2000 magnetic measurement device after being cleared off the residual diffusion sources. The melting temperatures of alloy ribbons were measured by differential scanning calorimeter (DSC, SDT Q600). Inductive coupled plasma optical electron spectroscopy (ICP-OES) was used to determine the overall composition of Tb in the magnets. Microstructural and compositional analyses were conducted by scanning electron microscopy (SEM, Carl Zeiss, Supra55) in back-scattered electron mode and electron probe microanalyzer (EPMA-1720H), respectively.

Fig. 1 shows the wettability and mobility of the TC, PTC, PTA and PTCA ingots over N50 substrates. The equilibrium contact angle (θ_{eq}) and equilibrium time (t_{eq}) are defined as corresponding angle and time in equilibrium state [17–19]. It is measured from Fig. 1(a) that θ_{eq} of PTCA/N50, PTA/N50 and PTC/N50 are 35°, 34° and 42°, respectively, obviously smaller than 63° of TC/N50. Furthermore, seen from Fig. 1(c–f), t_{eq} of PTCA/N50 and PTA/N50 are 46 s and 50 s, much shorter than 841 s of TC/N50 and 445 s of PTC/N50, respectively. It indicates that the mobility of PTA and PTCA over $Nd_2Fe_{14}B$ grains is much better than that of TC and PTC. The melting points of TC (746 °C), PTC (630 °C), PTA (632 °C) and PTCA (497 °C) ribbons determined by DSC are much lower than diffusion temperature at 900 °C [15]. The GBDP may follow these processes, in which diffusion alloys melt first and infiltrate into grain boundaries driven by concentration gradient as well as capillary force,

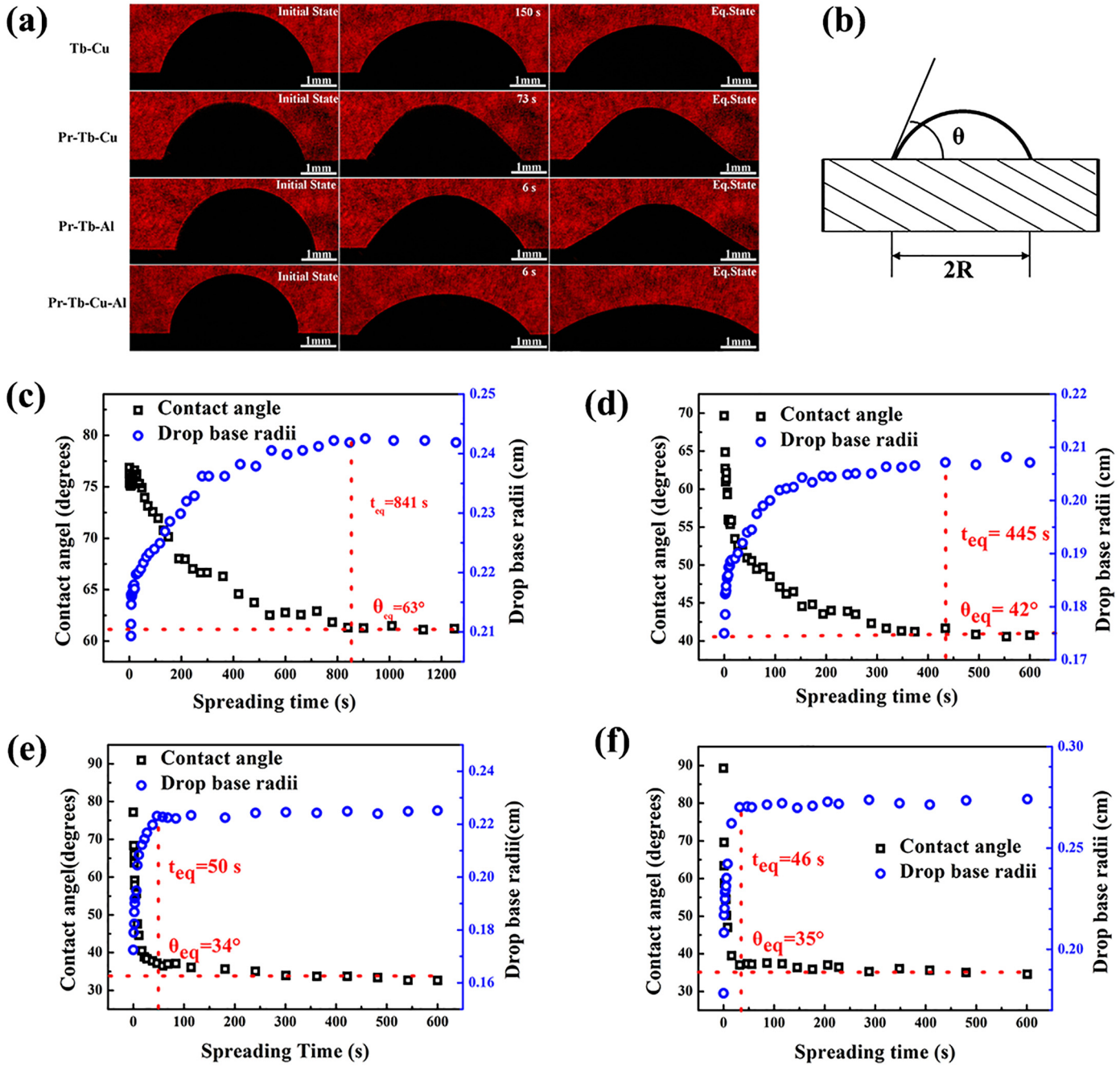

Fig. 1. (a) Representative photographs of TC, PTC, PTA and PTCA ingots on N50 substrates and (b) schematic illustration for contact angles θ and drop base radii R. The variations of contact angles θ and drop base radii R with time during isothermal dwells at 900 °C for the (c) TC, (d) PTC, (e) PTA and (f) PTCA alloys, respectively.